ORIGINAL ARTICLE

# Long noncoding RNA *lnc-RI* regulates DNA damage repair and radiation sensitivity of CRC cells through NHEJ pathway

**Ruixue Liu · Qingtong Zhang · Liping Shen · Shuangjing Chen · Junyan He · Dong Wang · Qi Wang · Zhenhua Qi · Meijuan Zhou · Zhidong Wang**

**Abstract** A percentage of colorectal cancer (CRC) patients display low sensitivity to radiotherapy, which affects its therapeutic effect. Cancer cells DNA double-strand breaks (DSBs) repair capacity is crucial for radiosensitivity, but the roles of long noncoding RNAs (lncRNAs) in this process are largely uncharacterized. This study aims to explore whether *lnc-RI* regulates CRC cell growth and radiosensitivity by regulating the nonhomologous end-joining (NHEJ) repair pathway. CRC cells in which *lnc-RI* has been silenced showed lower cell growth and higher apoptosis rates due to increased DSBs and cell cycle arrest. We

Ruixue Liu and Qingtong Zhang contributed equally to this work.

R. Liu · L. Shen · J. He · D. Wang · Q. Wang · Z. Qi ·
Z. Wang (✉)
Department of Radiobiology, Beijing Key Laboratory for
Radiobiology, Beijing Institute of Radiation Medicine, Beijing,
People's Republic of China
e-mail: wangzhidong_1977@aliyun.com

R. Liu
e-mail: liuruixue1109@163.com

L. Shen
e-mail: liping_shen@aliyun.com

J. He
e-mail: 304337839@qq.com

D. Wang
e-mail: wangdhh@foxmail.com

Q. Wang
e-mail: wqi619@126.com

Z. Qi
e-mail: tjuqzh@163.com

R. Liu · M. Zhou
Department of Radiation Medicine, Guangdong Provincial Key
Laboratory of Tropical Disease Research, School of Public Health,
Southern Medical University, Guangzhou, People's Republic of
China

M. Zhou
e-mail: lkzmj@smu.edu.cn

Q. Zhang
Department of Colorectal Surgery, Cancer Hospital of China
Medical University, Liaoning Cancer Hospital & Institute,
Shenyang, People's Republic of China
e-mail: 2690960111@qq.com

S. Chen
PLA Rocket Force Characteristic Medical Center, Beijing,
People's Republic of China
e-mail: chensj_1991@163.com

found that miR-4727-5p targets both *lnc-RI* and *LIG4* mRNA and inhibit their expression. CRC cells showed increased radiosensitivity when *lnc-RI* was silenced. These results reveal novel roles for *lnc-RI* in both DNA damage repair and radiosensitivity regulation in CRC cells. Our study revealed that *lnc-R*I regulates *LIG4* expression through *lnc-RI*/miR-4727-5p/*LIG4* axis and regulates NHEJ repair efficiency to participate in DNA damage repair. The level of *lnc-RI* was negatively correlated with the radiosensitivity of CRC cells, indicates that *lnc-RI* may be a potential target for CRC therapy. We also present the first report of the function of miR-4727-5p.

**Keywords** *Lnc-RI* · lncRNA · Non-homologous end-joining (NHEJ) · *LIG4* · *miR-4727-5p*

## Introduction

Colorectal cancer (CRC) is a predominant cancer with high incidence and mortality rates worldwide, especially in developed countries. Although many therapeutic methods for CRC have been developed in recent decades, there has been no significant improvement in the cure rate and long-term survival. Preoperative chemoradiotherapy is the conventional treatment for locally advanced CRC, but one-third of CRC patients display either low sensitivity or complete resistance to radiotherapy (Kawai et al. 2017; Baker et al. 2012). Identification of the molecular mechanisms that dictate radiation responses is of great clinical significance to CRC therapy.

The DNA damage response (DDR) is a precise surveillance system evolved to detect DNA damage and determine the fate of injured cells, and is one of the most vital fields in cancer biology (Nurse 1995) and other human diseases such as neurodegenerative diseases and aging (Katyal et al. 2014; López-Otín et al. 2013). DDR is often targeted to treat cancers, and it plays a critical role in chemo-/radiotherapy sensitivity regulation. It is commonly recognized that cancer cells with higher DNA repair activity possesses hyper resistance to radiochemotherapy (Goldstein and Kastan 2015). DNA damages occur when cells are subjected to genotoxic stresses. When exposed to ionizing radiation (IR), such as in the case of radiotherapy treatment of cancers, dominant lesions in vivo are the most catastrophic DNA double-strand breaks (DSBs).

Homologous recombination (HR) and non-homologous end-joining (NHEJ) are two main repair ways of DSBs. HR repair occurs during the S and G2 phases, and NHEJ plays a role throughout the cell cycle but more prominently in G1 cells (Dianatpour and Ghafouri-Fard 2017; Coutelier et al. 2018). Mammalian cells use NHEJ more frequently than HR in DSBs repair. NHEJ is an unusual DSBs repair pathway that joins the broken ends of DNA strands to prevent chromosome damage and thus preserving the viability of eukaryotic cells (Chang et al. 2017; Bartlett et al. 2016). Studies on DNA damage repair proteins is the key to DSBs repair related molecules. The core components in the NHEJ repair pathway include DNA-PK (a serine/threonine protein kinase) and its cofactors Ku70 and Ku80 holoenzymes, X-ray repair cross complementary protein 4 (XRCC4), and DNA Ligase4 (*LIG4*), which is essential for final "end-joining" (Jiang et al. 2013; Conlin et al. 2017).

Long noncoding RNAs (lncRNAs) refers to RNAs with length $\geq 200$ nt and lack meaningful open reading frames, accounting for about 4 to 9% of mammalian genome (Li et al. 2017). LncRNAs are known to play a critical role in a variety of biological processes, for example transcriptional co-activation, chromatin modifiers recruitment, miRNA sponges, splicing regulation, stability of gene expression, which are closely related to human disease occurrence, development, and prevention (Jiang et al. 2018; Davidovich and Cech 2015; Furió-Tarí et al. 2016; Ren et al. 2012; Zhao et al. 2018). It has been shown that some lncRNAs regulate DDR, and the majority of them are involved in HR repair, e.g., PCAT-1, DDSR1, and NORAD (Thapar 2018; Sharma et al. 2015; Munschauer et al. 2018), while for NHEJ repair, LINP1, a scaffold linking Ku80 and DNA-PKcs, is the most studied lncRNA in breast cancer (Zhang et al. 2016). However, the function of most lncRNAs in DDR is largely uncharacterized. In our previous studies, we found that *lnc-RI* is involved in regulation of HR in DSBs to maintain genomic stability (Shen et al. 2018). Whether *lnc-RI* could regulate the NHEJ pathway to improve DSBs repair was not studied. MicroRNAs (miRNAs) are endogenous non-coding RNAs of 20–24 nucleotides, which can inhibit the expression of genes by targeting mRNA 3'UTR or lncRNA sequences (Adlakha and Saini 2014; Chen et al. 2019).

In this research, we show that *lnc-RI* silencing inhibits CRC cell growth through increased DSBs and G1/

S arrest. *Lnc-RI* knockdown was found to suppress NHEJ efficiency and reduce *LIG4* expression. We found that in clinical CRC samples, *lnc-RI* expression is positively correlated with *LIG4* expression. We have also shown that *lnc-RI* competitively binds with miR-4727-5p to regulate *LIG4* mRNA stability and *lnc-RI* silencing enhanced CRC cells radiosensitivity. This study is the first report on *lnc-RI* in regulating NHEJ repair, a key pathway in DSBs repair. In addition, we revealed that *lnc-RI* regulates CRC radiosensitivity providing new insights for CRC therapeutics.

## Materials and methods

### Cell culture and irradiation

We purchased CRC cell lines (HCT116 and HT29 cells) from Chinese Academy of Sciences Cell Bank (China) and cultured them in a 37 °C cell incubator containing 5% CO2 and saturated humidity. HCT116 and HT29 cells were cultured in RPMI-1640 medium (HyClone, USA) and high-glucose DMEM medium (HyClone), respectively. In 100-μg/ml streptomycin (HyClone) and penicillin 100 units/ml, 10% fetal bovine serum (FBS) (ExCell Bio, China) should be added to the medium. The dose rate of $^{60}$Co γ-rays in CRC cells lines was 62.3 cGy/min at room temperature (25 °C).

### Lentiviruses, primers, and miRNA mimics

Lentiviruses expressing sequences of shRNA-*lnc-RI* or shRNA-NC (negative control) were packaged by GenePharma (China). Primers were synthesized by TsingKe Biological Technology (China) and miRNA mimics were synthesized by GenePharma. Sequences details are shown in Supplementary Information Tables S1.

### Lentivirus infection and the establishment of stable knockdown cell lines

CRC cell lines were infected with 20 multiplicity of infection (MOI) lentiviruses and 5 μg/ml of polybrene. After infected with lentiviral for 72 h, added puromycin (0.75 μg/ml) to the culture medium for 7 days to establish stable knockdown cell lines, the medium was then replaced with a concentration of 0.25 μg/ml puromycin.

### Transfection

Cells were transfected 24 h after inoculation. Lipofectamine 2000 (Invitrogen, USA) and jetPRIME® Transfection Reagent (Polyplus transfection, France) were used for transfection of miRNA mimics and plasmids, respectively.

### Cell proliferation assay

Cell proliferation was detected by cell counting kit-8 (CCK-8) colorimetric (Dojindo, Japan). Cells were inoculated in 96-well plates and treated after 24 h. Cell proliferation was determined at specific time points after infection. Experiments were performed on a minimum of four occasions. The 450-nm cell optical density (OD) was used to assess cell viability and was measured using a microplate reader (Sunrise, Switzerland).

### Clonogenic cell survival assay

Cells were inoculated in 6-well plates with $3 \times 10^5$ cells per well and reseeded into 6-well plates with lower density after infection or transfection. During cell culture, media was replaced every 3–5 days. After 2 weeks, the clones were fixed with methanol and stained with Giemsa. Microscopic colonies of more than 50 cells were thought to be effective, and the curves of surviving fractions using a multitarget/single-hit model (SF = 1–[1–e–D/D0] N) (Wang et al. 2018) counted the colonies manually, and an image scanner was used to get the original image.

### Xenograft assay

Animal experiments were carried out according to the ethical regulations permitted by the Animal Experiments Ethics Committee of Beijing Institute of Radiation Medicine. Female athymic nude mice aged 5–6 weeks were randomly assigned (Vital River, China; each group $n = 6$); food and water were provided ad libitum. Stable *lnc-RI* knockdown HCT116 cells ($1 \times 10^7$) were injected subcutaneously behind the thigh. Tumor was measured with digital caliper every 4 days, and the tumor volume was calculated using the following formula: volume = (length) × (width) × (width) × ($\pi$/6). After 30 days, subcutaneous tumors were removed and weighed.
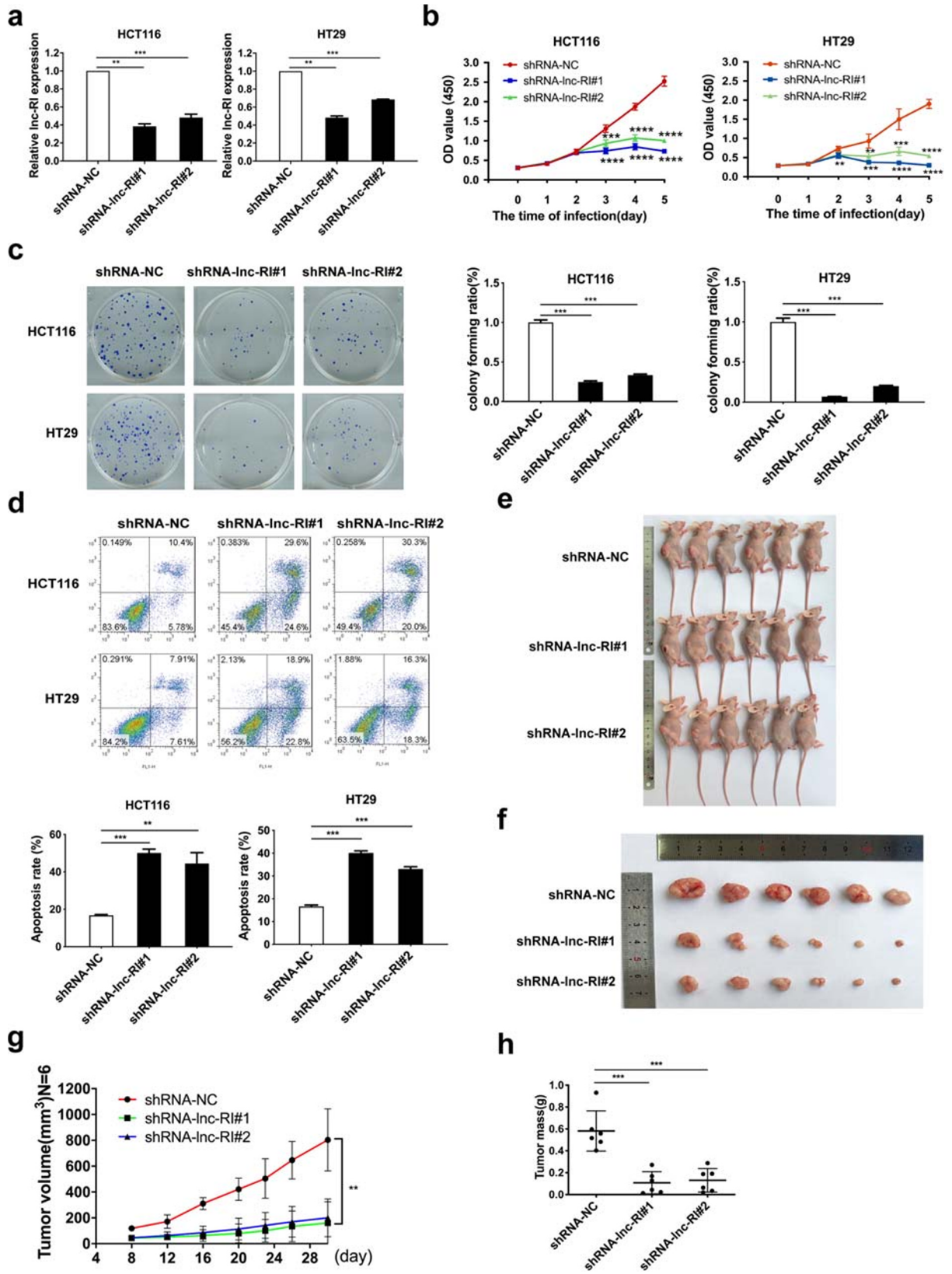
**Fig. 1** Loss of *lnc-RI* reduces CRC cell growth and viability. **a** ShRNA-mediated suppression of *lnc-RI* expression. Cells were infected with 20 MOI shRNA-*lnc-RI* or shRNA-NC. After 72 h, *lnc-RI* expression was detected by real-time PCR with GAPDH used as a loading control. t-test, mean ± SD, *n* = 3. **b** Knockdown of *lnc-RI* expression inhibited CRC cell proliferation. A total of 1000 cells were seeded in each well of a 96-well plate. After infection with either shRNA-*lnc-RI* or shRNA-NC, cell proliferation was measured with the CCK-8 assay at the indicated time points. *t* test, mean ± SD, *n* = 5. **c** *Lnc-RI* knockdown affected the rate of CRC cell clone formation. After infection with shRNA-*lnc-RI* and shRNA-NC, CRC cells were reseeded in 6-well plates and colony-formation assays were performed after 2 weeks. *t* test, mean ± SD, *n* = 3. **d** *Lnc-RI* knockdown aggravated CRC cell apoptosis. 72 h after infection with shRNA-*lnc-RI* and shRNA-NC, cells were collected and apoptosis detected by flow cytometry. *t* test, mean ± SD, *n* = 3. **e** and **f** BALB/c nude mice were subcutaneously injected with stable *lnc-RI* knockdown HCT116 cells and fed in an SFP grade environment. Tumor volume was measured every 4 days from day 8 of inoculation. Mice were sacrificed after 30 days and the tumors were excised. **g** *Lnc-RI* knockdown slowed tumor growth. Tumor volume (*n* = 6 tumors/group) was measured with an electronic Vernier caliper after injection. **h** Tumor was weighed after dissection, average tumor mass at day 30 is shown. *$P < 0.05$, **$P < 0.01$, ***$P < 0.001$, ****$P < 0.0001$

## Apoptosis analysis

Cells were harvested at 72 h after lentivirus infection. Apoptosis assay was performed according to the Annexin V-FITC apoptosis detection kits (Dojindo, Japan) instructions. Cells were analyzed by flow cytometry (BD FACS LSRII, USA), and at least, 10,000 cells were tested in each sample. Only Annexin V was positive for early apoptotic cells, both PI and Annexin V were positive for late apoptotic cells, while only PI was positive for necrotic cells. The total number of apoptotic cells is the sum of the number of early and late apoptotic cells.

## Cell cycle assay

Cells were treated 24 h after inoculation and harvested at a specified time point and were added with 70% (v/v) ethanol and place at − 20 °C overnight to fix the cells. After fixation, cells were washed twice with phosphate-buffered saline (PBS), added 200 μl PBS containing RNase (100 μg/ml) and PI (50 μg/ml), and incubated for 30 min at 37 °C. Cell cycle was detected by flow cytometry (ACEA Bio, USA). At least 10,000 events per sample were recorded.

## RNA extraction and real-time quantitative PCR (RT-qPCR)

Trizol reagent (Sigma, USA) was used to extract total RNA from cells, and ultraviolet spectrophotometer (GE Healthcare GeneQuant 100, USA) was used to determine the concentration and purity of RNA. The PrimeScriptRT reagent kit (TaKaRa, Japan) was used for reverse transcription; 1-μg total RNA was reversely transcribed into cDNA from each sample. RNA expression was detected by RT-qPCR, using the iTaq™ Universal SYBR Green Supermix (Bio-Rad; USA). The experiment was repeated three times, and GAPDH was used as control gene to calculate the relative expression (2-ΔΔCt).

## Gene chip assay

The gene chip assay was completed with the assistance of the company Premedical Laboratories Co., Ltd. The PrimeView™ Human Gene Expression Array was used in this study, which included preparation of chip and sample, hybridization reaction, and signal detection. Genes with a fold change of greater than 1.2 times are considered to be differentially expressed genes.

## Clinical sample acquisition

CRC clinical samples were obtained from the department of Colorectal Surgery, Liaoning Cancer Hospital. Forty-eight cases were used, 19 males and 29 females, aged between 29 and 81 years. All patients were diagnosed with CRC, and the cancer and adjacent tissues were obtained during surgery. The experiment was conducted with the informed consent of patients and reviewed by the ethics committee of Liaoning Cancer Hospital.

## Protein extraction and Immunoblotting

Samples were harvested and washed twice in precooled PBS, added lysis buffer containing phosphatase and protease inhibitors (Roche Applied Science, USA) to lyse cells in an ice bath, and centrifuged at 4 °C. Protein concentration was detected using BCA Assays (Beyotime Biotechnology, China). SDS sample buffer was added to the supernatant to denature the protein, resolved by SDS-polyacrylamide gel electrophoresis, and transferred to nitrocellulose membranes. Primary
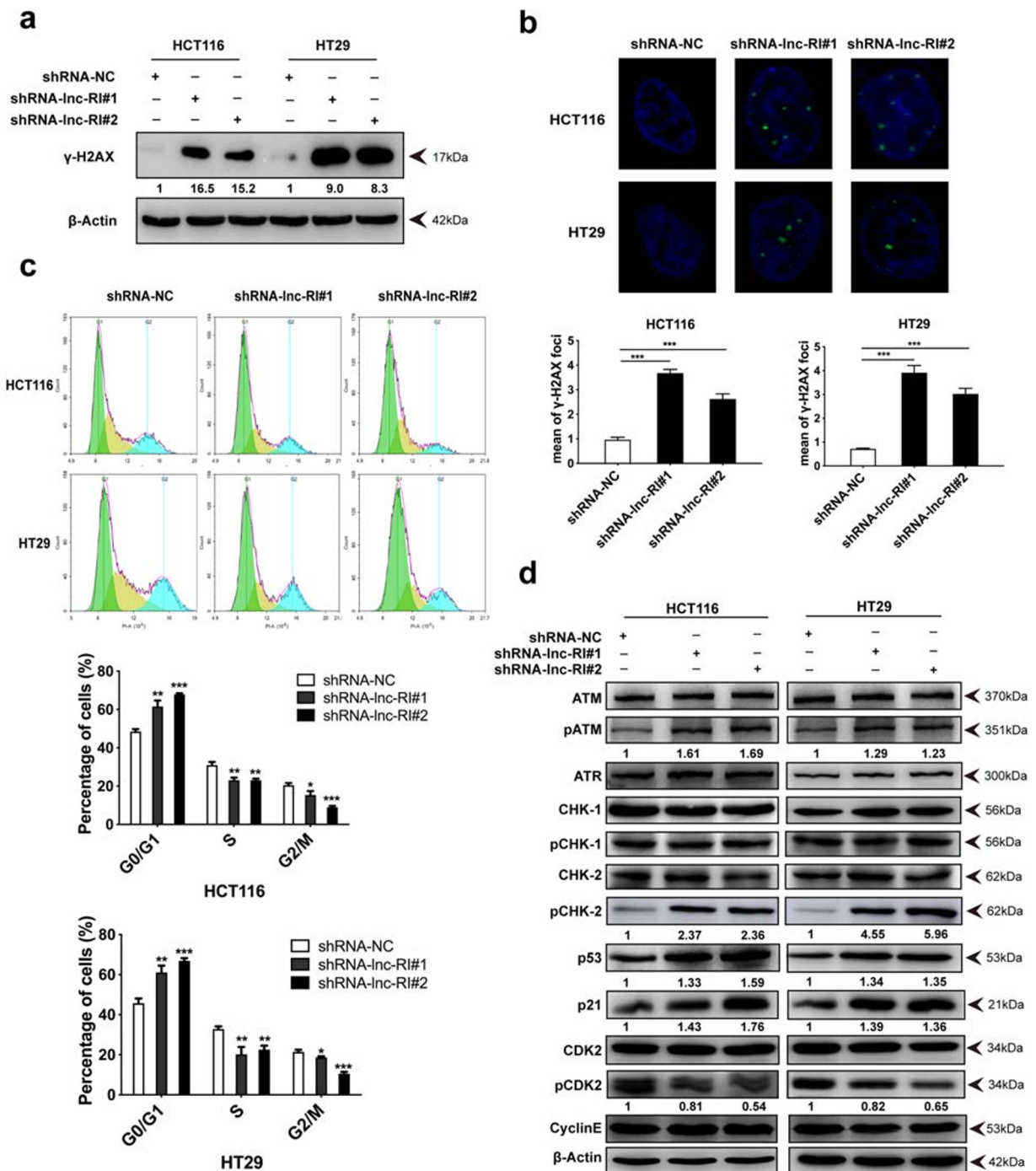
Fig. 2 Absence of *lnc-RI* induces CRC cells DSBs and induces G1/S phase arrest through the ATM- > p53- > p21- > Cyclin E-CDK2 pathway. **a** *Lnc-RI* knockdown increased γ-H2AX expression. CRC cells were collected 72 h after infection with shRNA-*lnc-RI* or shRNA-NC. γ-H2AX expression was detected by Western blot analysis. **b** *Lnc-RI* knockdown triggers γ-H2AX foci formation. CRC cells were seeded onto coverslips in six-well plates and infected with shRNA-*lnc-RI* or shRNA-NC for 72 h. γ-H2AX foci were detected by indirect immunofluorescence staining, 200 randomly selected cells in each group

were counted. *t* test, mean ± SD, *n* = 200. **c** *Lnc-RI* knockdown induced G1/S arrest. CRC cells were infected with shRNA-*lnc-RI* or shRNA-NC for 72 h, and the cell cycle was detected by flow cytometry. A total of 10,000 cells in each sample were scored. *t* test, mean ± SD, *n* = 3. **d** *Lnc-RI* knockdown activated the ATM- > p53- > p21- > Cyclin E-CDK2 pathway. CRC cells were collected 72 h after infection with shRNA-*lnc-RI* or shRNA-NC. The expression of related proteins in this pathway was detected by Western blot analysis. $*P < 0.05$, $**P < 0.01$, $***P < 0.001$

antibodies against β-actin (60008–1-lg; Proteintech), γ-H2AX ser139 (05–636; Millipore), ATM (sc-23,921; Santa Cruz), pATM S1981 (ab81292; Abcam), ATR (13934S; Cell Signaling), CHK1 (sc-8408; Santa Cruz), pCHK1 Ser345 (2341S; Cell Signaling), CHK2 (sc-5278; Santa Cruz), pCHK2 Thr68 (2197S; Cell Signaling), p53 (sc-126; Santa Cruz), p21 (sc-6246; Santa Cruz), CDK2 (ab32147; Abcam), pCDK2 (ab194868; Abcam), cyclinE (sc-248; Santa Cruz), DNA-PKcs (19983–1-AP; Proteintech), *LIG4* (12695–1-AP; Proteintech), KU70 (ab3114; Abcam), and KU80 (ab80592; Abcam). Membranes were labeled with the appropriate secondary antibodies (KPL, USA) conjugated to horseradish peroxidase (HRP). The Image Quant LAS 500 system (GE Healthcare, USA) was used for visualization of protein bands.

## Immunofluorescence assays

Cells were cultured on polylysine-treated coverslips. At 72-h post-infection, cells were added with 4% paraformaldehyde to fix cells, 0.3% Triton X-100-PBS buffer to permeate the cells. Three percent bovine serum albumin (BSA) was used to block cells. And then incubated cells with antibodies against γ-H2AX (1:400) and FITC-labeled anti-IgG antibodies (1:400; KPL), respectively. DNA was stained using 4, 6-diamidino-2-phenylindole (DAPI). Nikon Ti-A1 capture system was used to acquire images. Representative images are shown. Each group randomly selected 200 cells and manually counted the γ-H2AX foci in the nucleus.

## NHEJ repair efficiency assay

Stable *lnc-RI* knockdown cell lines were transfected with 0.5-μg linearized EJ5-GFP (digested with Hind III), linearized NHEJ-GFP plasmids were involved in NHEJ repair showed as GFP-positive (GFP+) cells. Cells were harvested after 48 h and NHEJ repair efficiency detection via fluorescence-activated cell sorting (FACS).

## Dual luciferase reporter assay

The sequences (1-151 bp) of *LIG4* mRNA 3′-untranslated region (3′UTR) and partial *lnc-RI* sequences (1140-1364 bp) were inserted into pmirGLO vector, which expresses renilla and firefly luciferase to generate pmirGLO-*LIG4*/*lnc-RI*-3′UTR-wt constructs. The

sequence of binding site mutations was inserted into pmirGLO vector, to generate pmirGLO-*LIG4*/*lnc-RI*–3′UTR-mu constructs. Plasmids were synthesized by TsingKe Biological Technology. After 8 h of cell transfection with 80 ng reporter or pmirGLO plasmid, 100 nM miR-4727-5p mimic or miR-NC were transfected. The luciferase activity of the cells was detected by Dual-Luciferase Reporter Assay System (Promega, USA). Firefly luciferase activity was normalized to renilla luciferase.

## Statistical analysis

Data were presented as mean ± standard deviation (all experiments were repeated three times). Two-tailed Student's *t* test was used for data comparison (*$P < 0.05$, **$P < 0.01$, ***$P < 0.001$, or **** $P < 0.0001$ was considered statistically significant). Error bars indicate s.e.m.

# Results

## *Lnc-RI* silencing reduces the growth and viability of CRC cells

As shown in Fig. 1a, the lentiviral vector expressing shRNA-*lnc-RI*#1/2 effectively reduced *lnc-RI* expression in CRC cells. We performed CCK-8 assays to assess cell proliferation from 0- to 5-day postsilencing, and found that *lnc-RI* silencing restrained CRC cells proliferation (Fig. 1b). We further verified *lnc-RI* effect on the growth of CRC cells through clonogenic assays. As expected, following infection with shRNA-*lnc-RI*, CRC cells colony-forming ratio was significantly reduced (Fig. 1c). We next explored the role of *lnc-RI* in apoptosis. At 72 h postinfection, cells were tested by flow cytometric analysis of Annexin V–conjugated FITC/PI staining. The proportions of apoptotic cells were significantly increased after *lnc-RI* silencing (Fig. 1d). To explore the effects of *lnc-RI* silencing in vivo, we subcutaneously injected BALB/c Nude mouse with *lnc-RI* stably silenced cell lines. *Lnc-RI* silencing causes a significantly reduced rate of xenograft tumor growth over 30 days (Fig. 1e–f). A three-fold change in tumor volume was observed between shRNA-NC and shRNA-*lnc-RI* tumors as early as 12 days post-injection and reached 4–5-fold
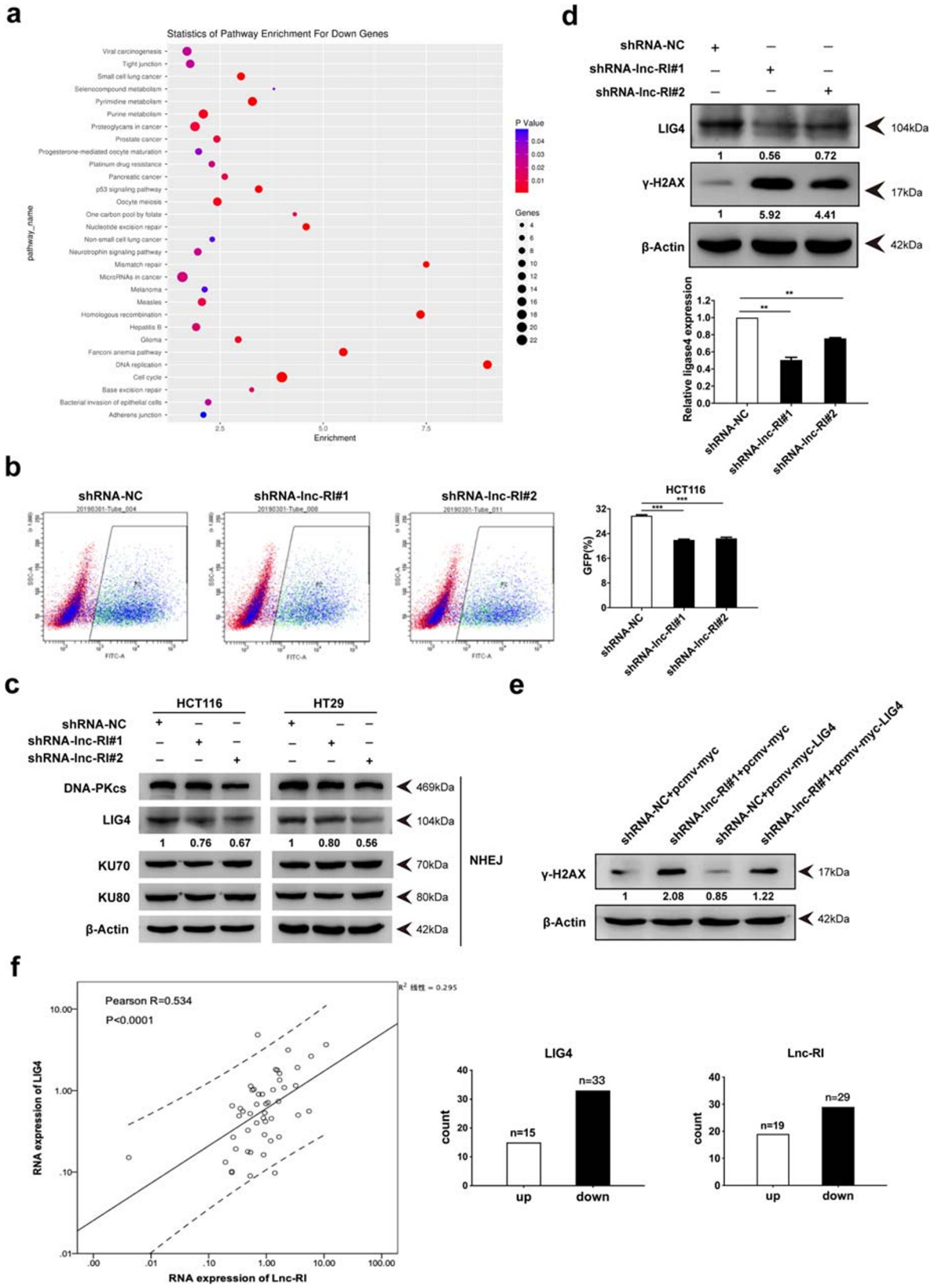
◀ **Fig. 3** *Lnc-RI* affects NHEJ repair efficiency by regulating *LIG4* expression. **a** Gene chip results showed that knocking down *lnc-RI* affected the DNA damage repair pathway. Signal pathway analysis of downregulated genes functional enrichment. **b** *Lnc-RI* knockdown suppressed NHEJ pathway efficiency. Stable *lnc-RI* knockdown HCT116 cells were transfected with 0.5 μg of linearized NHEJ-GFP reporter plasmid. GFP-positive (GFP+) cells represent the linearized NHEJ-GFP plasmids joined by the NHEJ of DSBs repair. *t* test, mean ± SD, *n* = 3. **c** Lack of *lnc-RI* affected the NHEJ pathway proteins for DSBs repair. CRC cells were infected with shRNA-*lnc-RI* or shRNA-NC, and the expression of pathway related proteins were detected by Western blot analysis. **d** Knockdown of *lnc-RI* suppressed *LIG4* expression. HCT116 cells were infected with shRNA-*lnc-RI* or shRNA-NC for 72 h. *LIG4* mRNA and protein was detected by real-time PCR (bottom) and Western blot (top), respectively. *t* test, mean ± SD, *n* = 3. **e** *LIG4* overexpression can reverse the damage caused by knocking down *lnc-RI*. HCT116 cells were infected with shRNA-*lnc-RI* or shRNA-NC, and transfected with the *LIG4* overexpression plasmid for 48 h. γ-H2AX expression was detected by Western blot analysis. **f** *Lnc-RI* is positively relative to *LIG4* expression in 48 clinical CRC samples. The expression of *lnc-RI* and *LIG4* was detected by real-time PCR. *$P < 0.05$, **$P < 0.01$, ***$P < 0.001$

after 30 days (Fig. 1g). The tumor weights in the shRNA-*lnc-RI* group were lower than the shRNA-NC group (Fig. 1h). These data suggested that *lnc-RI* plays an important role in CRC cells growth and apoptosis.

*Lnc-RI* silencing induces CRC cells DSBs and induces G1/S phase arrest through the ATM- > p53- > p21- > Cyclin E-CDK2 pathway

In CRC cells, we found that *lnc-RI* silencing in HCT116 and HT29 cells for 72 h increased γ-H2AX protein levels and foci formation which suggests the induction of DSBs (Fig. 2a, b). DNA damage can trigger G1/S or G2/M arrest as a protective response to allow cells time to repair prior to cell division (Barshishat et al. 2018). We found that upon *lnc-RI* silencing for 72 h, HCT116 and HT29 cells showed G1/S arrest (Fig. 2c). One of the dominant checkpoint responses to DSBs through the G1 phase is the ATM/ATR- > p53- > p21- > Cyclin E-CDK2 pathway, which targets the G1/S promoting cyclin E/CDK2 kinase (Nurse 1995). Upon assessment of the known cell cycle markers, we found that *lnc-RI* silencing led to increased levels of pATM, p53, and p21 and decreased levels of pCDK2 compared with the control group, and that the increase of pCHK2 protein levels can promote p53 activation (Fig. 2d).

According to published studies, a loss of CDK2 expression prevents G1 to S phase transition (Dai et al. 2013). In previous studies, we found that *lnc-RI* silencing in Hela cells resulted in G2/M as opposed to G1/S phase arrest (Wang et al. 2016). We believe the cell cycle arrest differences between different cells in which *lnc-RI* is silenced may be due to p53 expression levels. Firstly, we silenced *lnc-RI* and assessed cell cycle progression in HCT116, a p53-deficient cell line. We saw no G1/S arrest in the shRNA-*lnc-RI*#1 group, and lower levels of G1/S arrest in the shRNA-*lnc-RI*#2 group compared with HCT116 control cells (Fig. S1a). Next, we investigated p53 level in Hela and CRC cells, and found that p53 level in CRC cells was higher than Hela cells (Fig. S1b). Last, we confirmed that *lnc-RI* silencing in HCT116 p53-deficient cells induced DNA damage but did not activate p21 (Fig. S1c). Taken together, these data suggest that the G1/S arrest caused by *lnc-RI* silencing is associated with p53.

*Lnc-RI* regulates NHEJ repair efficiency by stabilizing *LIG4* expression

To explore the molecular mechanism of DSBs induced by *lnc-RI* silencing, we used gene chip technology to screen differentially expressed genes (DEGs) in shRNA-NC and shRNA-*lnc-RI* groups, to provide a basis for the selection of downstream target genes (Fig. 3a and Fig. S2). Signal pathway enrichment analysis showed that pathways enriched in downregulated DEGs were closely related to DNA damage repair. The expression of RAD51, BRCA1, MRE11, and *LIG4* are all downregulated. We have proved that knockdown of *lnc-RI* could inhibit DSBs HR repair by reducing RAD51 expression in previous study (Shen et al. 2018). We then wanted to examine whether *lnc-RI* plays a role in DSBs NHEJ repair. We detected NHEJ efficiency in HCT116 cells through the EJ5-GFP reporter system. The GFP-positive (GFP+) percentage represents NHEJ repair efficiency and detected by FACS. As shown in Fig. 3b, NHEJ repair efficiency was significantly inhibited in stable *lnc-RI* knockdown cell lines. Upon assessment of NHEJ repair pathways, we found that *LIG4* expression decreased following *lnc-RI* silencing (Fig. 3c). In addition to these observations, *lnc-RI* silencing significantly inhibited *LIG4* mRNA and protein level (Fig. 3d), and the exogenous expression of *LIG4* protected against the DNA damage observed following *lnc-RI* silencing (Fig. 3e). We also
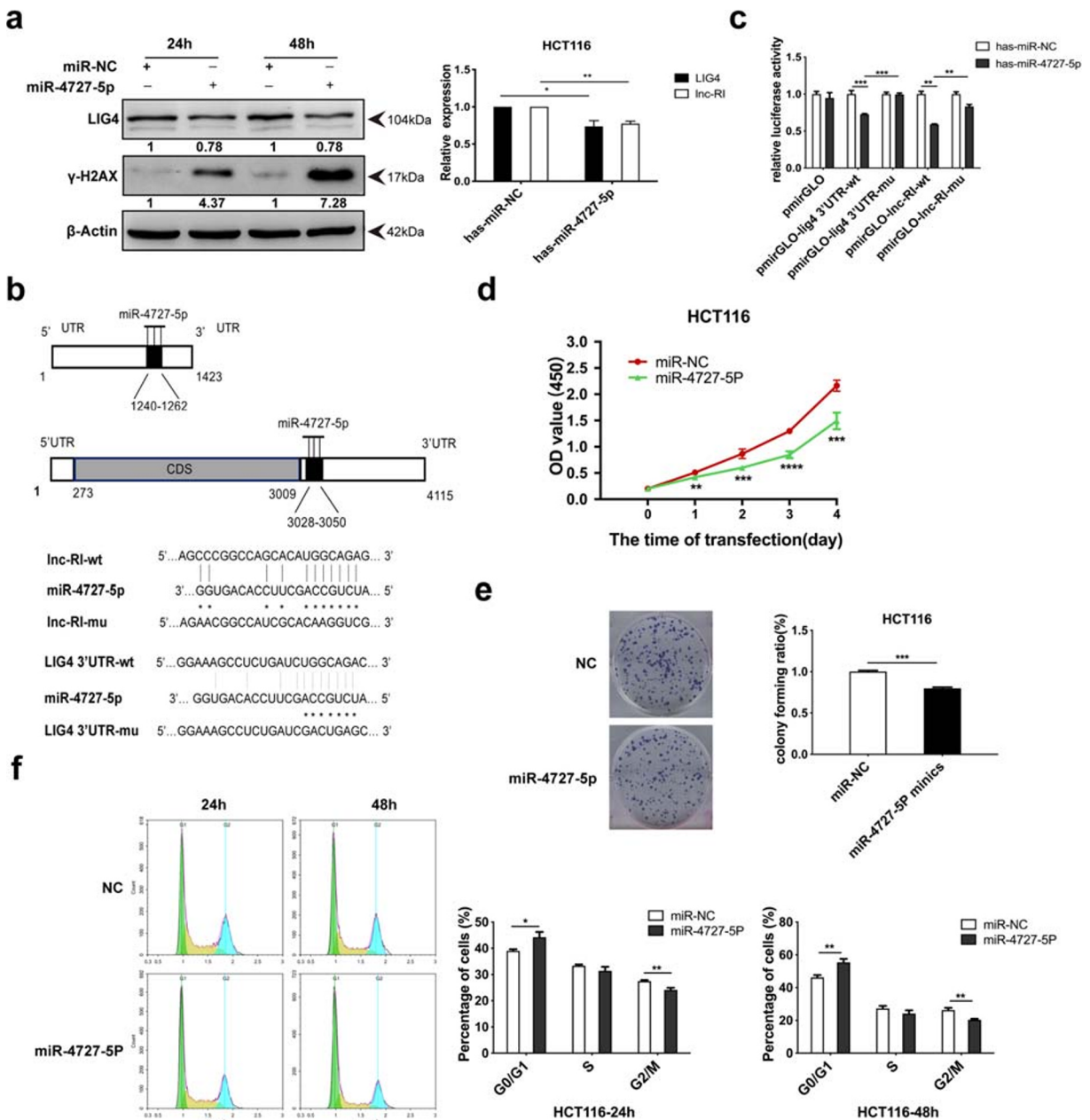
Fig. 4 *Lnc-RI* regulates *LIG4* through competitive binding with miR-4727-5p. **a** MiR-4727-5p mimics decreased *lnc-RI* and *LIG4* mRNA and protein levels. HCT116 cells were treated with miR-4727-5p mimics for 48 h, and the relative expression of *lnc-RI* and *LIG4* were detected by real-time PCR. *t* test, mean ± SD, *n* = 3. Western blot analysis of *LIG4* and γ-H2AX proteins expression in HCT116 cells following treatment with miR-4727-5p mimics for 24 and 48 h. **b** Predicted miR-4727-5p target sites in *lnc-RI* and *LIG4* mRNA 3′UTR. Luciferase reporter vectors were constructed by cloning the wild-type and mutated *LIG4* mRNA 3′UTR/*lnc-RI* sequences targeted by miR-4727-5p into pmirGLO plasmids. **c** MiR-4727-5p directly targeted *lnc-RI* and *LIG4* mRNA 3′UTR. HCT116 cells were cotransfected with the reporter vectors and miR-4727-5p mimics or NC. Luciferase activity was measured at 48 h after transfection. *t* test, mean ± SD, *n* = 3. **d** MiR-4727-5p mimics inhibited cell proliferation. HCT116 cells were seeded in 96-well plates (1000 cells of each well), after transfection with miR-4727-5p mimics, a CCK-8 assay was performed to analyze cell proliferation at the indicated time points. *t* test, mean ± SD, *n* = 5. **e** MiR-4727-5p mimics reduced the rate of cell clone formation. After transfection with miR-4727-5p mimics, HCT116 cells were reseeded in 6-well plates and colony-formation assays were conducted after 2 weeks. *t* test, mean ± SD, *n* = 3. **f** MiR-4727-5p mimics induced cell cycle arrest. Cell cycle analysis was performed by flow cytometry after HCT116 cells were transfected with miR-4727-5p for 24 and 48 h. *t* test, mean ± SD, *n* = 3. *\*P* < 0.05, *\*\*P* < 0.01, *\*\*\*P* < 0.001, *\*\*\*\*P* < 0.0001

confirmed that *lnc-RI* expression is positively correlated with *LIG4* expression in 48 clinical CRC samples (Pearson $R = 0.534$, $P < 0.0001$) following RT-qPCR analysis (Fig. 3f), *lnc-RI* expression was increased in 19 and decreased in 29 cases, and *LIG4* was highly expressed in 15 and poorly expressed in 33 cases. These data suggest that *lnc-RI* regulates the NHEJ repair pathway by stabilizing *LIG4* expression.

*Lnc-RI via competitive binding with miR-4727-5p to regulates LIG4*

It is well-known that there are a range of lncRNAs can be used as competitive endogenous RNAs (ceRNAs) to stabilize target genes. We explored miRNAs that can target both *LIG4* mRNA 3′UTR and *lnc-RI* through open database predictions (TargetScan, RegRNA2.0, miRDB, microRNA.org-Targets and Expression, and miRTarBase). Six miRNAs were screened, including miR-6817-5p, miR-3662, miR-1587, miR-3620-5p, miR-4727-5p, and miR-4769-3p. We assessed the effects of miRNA mimics on *LIG4* and γ-H2AX levels, and observed that miR-4727-5p mediated the most significant inhibition of *LIG4* expression, with a concomitant increase of γ-H2AX (Fig. S3). As shown in Fig. 4 a, transfection with miR-4727-5p mimics reduced *lnc-RI* and *LIG4* mRNA expression, and significantly increased γ-H2AX expression. To confirm miR-4727-5p's direct interactions with *lnc-RI* and *LIG4*, we constructed pmirGLO-*lnc-RI*-wt/mu, pmirGLO-*LIG4*-3′ UTR-wt/mu reporter vectors (Fig. 4b). Either miR-4727-5p mimics or miR-NC were cotransfected with these reporter vectors. As can be seen in Fig. 4c, miR-4727-5p inhibited pmirGLO-*lnc-RI*/*LIG4*-wt reporters luciferase activity and had no effects on pmirGLO-*lnc-RI*/*LIG4*-mu reporters. Therefore, miR-4727-5p can directly acts on *lnc-RI* and *LIG4* mRNA 3′UTR to regulate their expression. We then transfected miR-4727-5p mimics into HCT116 cells and performed CCK-8 assays to assess cell proliferation. Figure 4d shows that miR-4727-5p significantly inhibited HCT116 cell proliferation. We further examined miR-4727-5p effects on colony formation and the cell cycle status of HCT116 cells. The colony number of miR-4727-5p was lower than miR-NC group (Fig. 4e), and cell cycle arrest was observed (Fig. 4f). These data suggest that the cytological phenotype induced by the miR-4727-5p mimics was consistent with that observed in response to *lnc-RI* silencing.

**Table 1** The main parameters of a multi-target model based on colony formation assays

|  | N | D0 | Dq | SER |
|---|---|---|---|---|
| HCT116-shRNA-NC | 1.999 | 1.408 | 0.976 | |
| HCT116-shRNA-*lnc-RI*#1 | 2.078 | 1.046 | 0.765 | 1.275 |
| HCT116-shRNA-*lnc-RI*#2 | 1.980 | 1.168 | 0.798 | 1.222 |
| HT29-shRNA-NC | 2.300 | 1.488 | 1.239 | |
| HT29-shRNA-*lnc-RI*#1 | 2.131 | 0.953 | 0.721 | 1.718 |
| HT29-shRNA-*lnc-RI*#2 | 1.892 | 1.218 | 0.777 | 1.596 |

*N*, extrapolation number; *D0*, mean lethal dose; *Dq*, quasi-threshold dose; *SER*, sensitivity

*Lnc-RI is negatively correlated with CRC cell radiosensitivity*

DNA damage repair is closely related to cancer cell radiosensitivity (Hatano et al. 2015; Thangavel et al. 2014). *Lnc-RI* silencing induced DSBs in CRC cells (Fig. 2a, b), so we predicted that *lnc-RI* expression is negatively correlated with CRC cell radiosensitivity. As previously observed, HT29 cells display higher chemo- and radiation resistance than HCT116 cells (Spagnoletti et al. 2018; Urick et al. 2011), results that were confirmed in our study (Fig. 5a and Fig. S4). We found that *lnc-RI* and *LIG4* expression in HT29 cells were higher than that in HCT116 cells (Fig. 5b). In addition, we performed DSBs detection on CRC cells after 4 Gy irradiation, including γ-H2AX foci analysis and γ-H2AX protein expression. The results (Fig. 5c, d) indicated that HT29 cells showed less damage than HCT116 cells after IR treatment. Finally, following *lnc-RI* silencing, we observed clonogenic ability at different radiation doses 0, 1, 2, and 4 Gy in CRC cells and based on clonogenic survival assays calculated the parameters of a multitarget/single-hit model. The results (Fig. 5e, Table 1 and Fig. S5) indicated *lnc-RI* silencing increased radiosensitivity in CRC cells, and that the radiation sensitization was more pronounced in HT29 than HCT116 cells, which confirmed its role in CRC cell radiosensitivity.

## Discussion

Emerging evidence reveals that lncRNAs play key roles in various life processes and in the development of human disease (Jiang et al. 2018; Davidovich and Cech 2015; Furió-Tarí et al. 2016; Ren et al. 2012; Zhao et al.
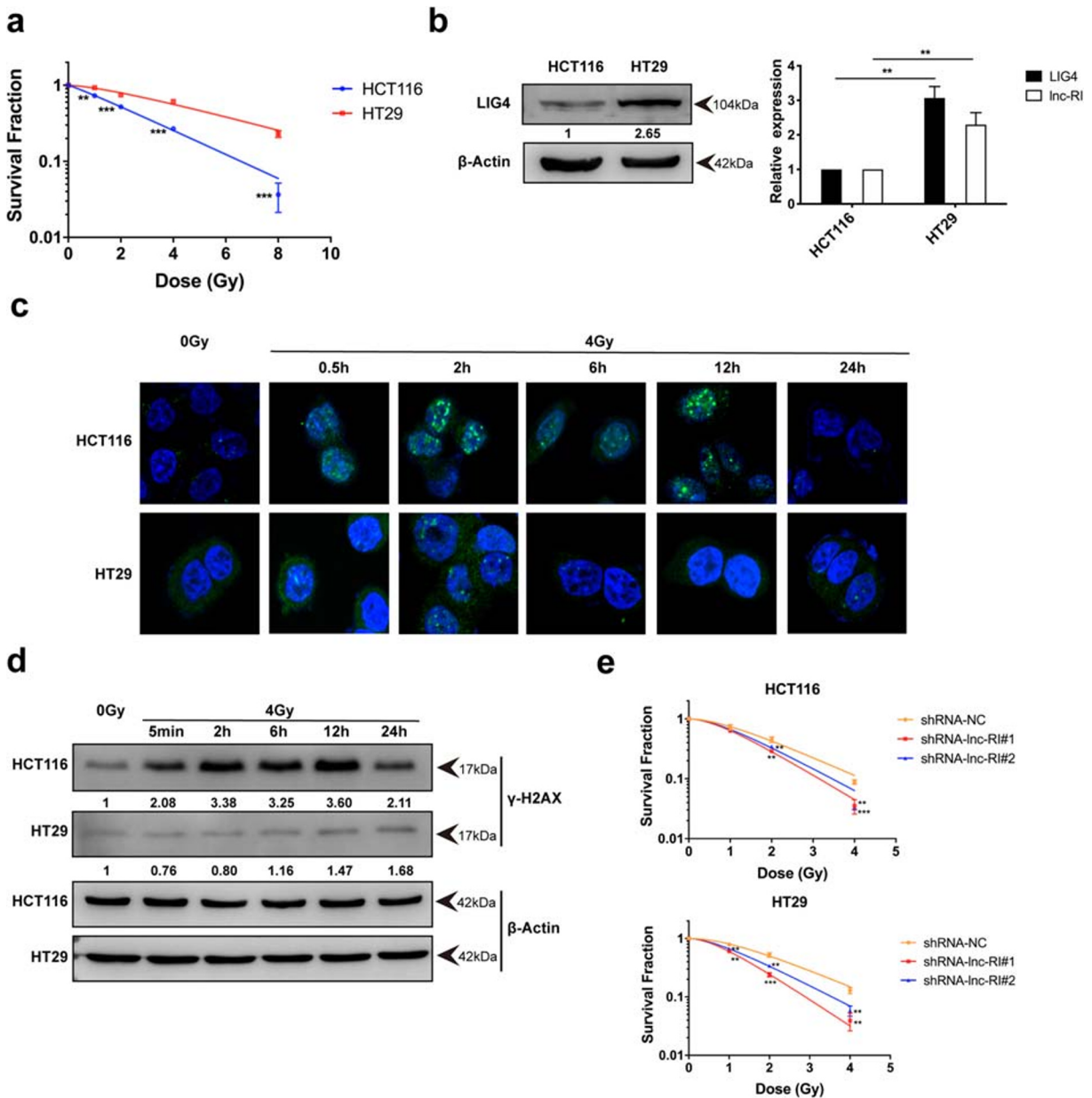
Fig. 5 *Lnc-RI* is negatively correlated with CRC cell radiosensitivity. **a** HCT116 cells are more sensitive to IR than HT29 cells. HCT116 and HT29 cells were seeded into 6-well plates, and colony-formation assays were performed after irradiation (0, 1, 2, 4, 8Gy). *t* test, mean ± SD, *n* = 3. **b** *LIG4* protein level in HT29 cells was significantly higher than that in HCT116 cells. The expression of *LIG4* protein was detected by Western blot analysis. The expression levels of *lnc-RI* and *LIG4* in HT29 cells were higher than those in HCT116 cells. Relative expression of *lnc-RI* and *LIG4* were detected by real-time PCR. *t* test, mean ± SD, *n* = 3. **c** Numbers of γ-H2AX foci were higher in HCTT16 cells than HT29 cells after the same IR dose. Cells were inoculated in

coverslips in six-well plates and fixed at the specified time points after 4Gy irradiation. γ-H2AX foci were detected by indirect immunofluorescence staining. **d** γ-H2AX protein level increased significantly after IR in HCT116 cells compared to HT29 cells. Cells were harvested at the indicated time points after 4Gy irradiation. γ-H2AX protein was detected by Western blot analysis. **e** *Lnc-RI* knockdown enhanced CRC cell radiosensitivity. After infection with shRNA-*lnc-RI* and shRNA-NC, CRC cells were inoculated in 6-well plates and colony-formation assays were performed after irradiation. *t* test, mean ± SD, *n* = 3. \**P* < 0.05, \*\**P* < 0.01, \*\*\**P* < 0.001
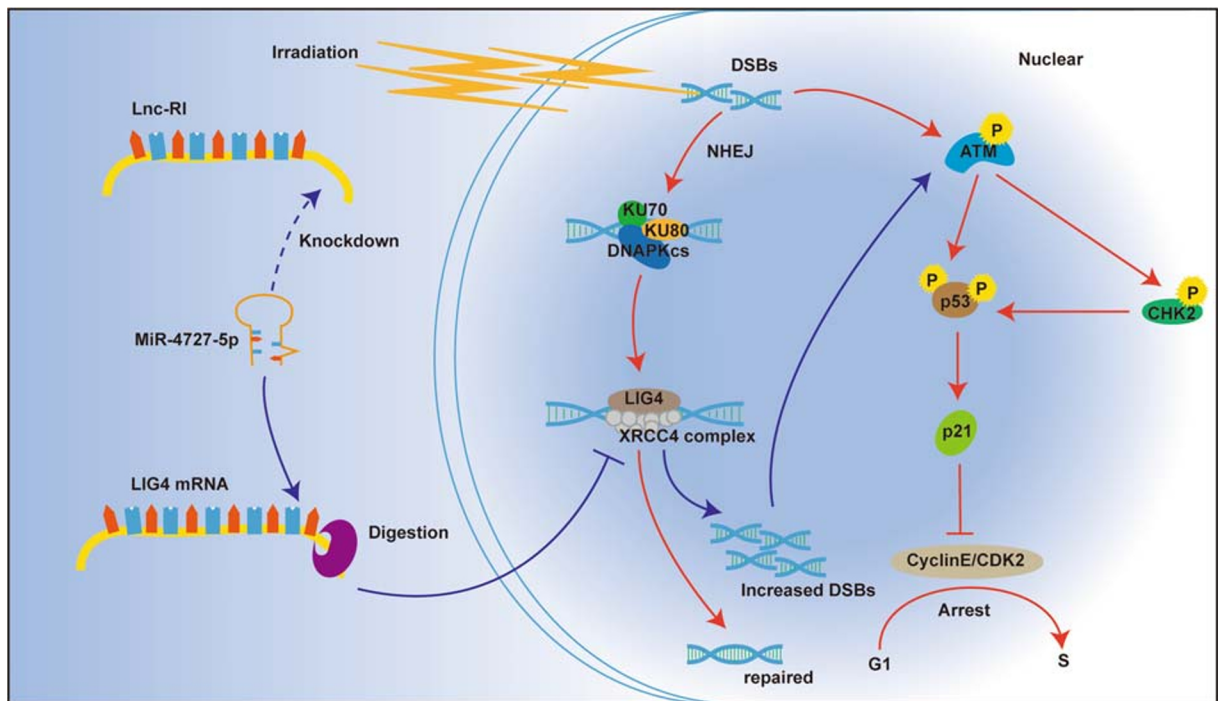
**Fig. 6** Schematic of the interaction between miR-4727-5p and *lnc-RI*/*LIG4* in the regulation of NHEJ and DSBs

2018). Very few lncRNAs are reported to have NHEJ functions with LINP1 being the most famous NHEJ-related lncRNA, which is expected to be an important target for breast cancer treatment (Zhang et al. 2016). However, studies regarding lncRNA involvement in the NHEJ pathway remain limited. In this study, we found an essential lncRNA *lnc-RI* in NHEJ regulation. We demonstrated that *lnc-RI* plays a novel role in NHEJ pathway during DSBs repair, and is negatively correlated with radiosensitivity in CRC cells. We showed that *lnc-RI* via the *lnc-RI*/miR-4727-5p/ *LIG4* axis as a ceRNA to regulate *LIG4* expression, thereby affecting the NHEJ repair efficiency and radiation sensitivity.

DSBs emerge from radiation, chemical induction, reactive oxygen species, and harmful metabolites. NHEJ is the predominant repair pathway that occurs during cell cycle progression to restore the duplex structures caused by DSBs. NHEJ requires nucleases to remove DNA lesions, polymerases to replace the damaged DNA, and ligases to restore DNA integrity (Lieber 2010). The NHEJ repair pathway includes KU70/KU80, DNA-PKcs, *LIG4*, XRCC4, XLF and Artemis, and *LIG4* is considered essential for final "end-joining". *LIG4* dysfunction results in NHEJ deficiency leading to developmental delay, radiosensitivity,

neurodegeneration, carcinogenesis, and immunodeficiency (Lieber et al. 2003; O'Driscoll et al. 2004).

In this research, we confirmed that *lnc-RI* silencing significantly inhibited CRC cell growth and promoted apoptosis. These effects were mediated through increased DSBs in silenced CRC cells leading to G1/S phase arrest by activating the ATM- > p53- > p21- > Cyclin E-CDK2 pathway (Foster et al. 2012). Following DNA repair, cells that repair correctly can enter the cell cycle while those that fail to repair initiate apoptotic mechanisms. Our data indicates that *lnc-RI* silencing suppresses NHEJ repair efficiency. Intriguingly, we found that *LIG4* expression, a key molecule in the NHEJ repair pathway, decreased at both the mRNA and protein level. Among the 48 clinical samples, 36 showed the same expression *lnc-RI* and *LIG4* trends in cancer tissue, compared with adjacent tissue, providing direct evidence for our cell based results. LncRNAs are used as bait for miRNAs to regulate target gene expression (Chen et al. 2018; Zhu et al. 2017). We screened miRNAs targeting both *lnc-RI* and *LIG4* mRNA 3'UTR through public database predictions, and found that miR-4727-5p mimics inhibited *lnc-RI* and *LIG4* expression and enhanced γ-H2AX expression. And this is the first report to demonstrate the molecular

mechanism of miR-4727-5p. Furthermore, the direct interactions between miR-4727-5p and target sites in the 1240–1262 bp region of *lnc-RI* and the 3'UTR 3028–3050 bp region of *LIG4* mRNA were confirmed by dual luciferase reporter assays. This confirmed that *lnc-RI* through competitive binding with miR-4727-5p to regulate *LIG4* expression. We speculate that *LIG4* silencing was consistent with the effect of miR-4727-5p mimics on cell survival, but this requires further study to confirm and characterize.

LncRNAs are used as biomarkers or therapeutic targets, providing new insight for tumor diagnosis and treatment (Giraldez et al. 2019; Sole et al. 2019; Martens-Uzunova et al. 2014; Yu et al. 2015). It is increasingly clear that DSBs repair capacity is a key factor of radiosensitivity in tumor radiotherapy (Rube et al. 2008; Tarish et al. 2015). Inhibiting the ability of tumors to repair is an important direction for the development of anticancer therapeutics (Pounami Samaddera et al. 2016). We propose that *lnc-RI* has potential value in the evaluation of chemo-/radiosensitivity of CRC cells. As a caveat, the lack of clinical research regarding *lnc-RI* limits its clinical application for the time being.

In summary, our results indicate that the *lnc-RI* closely associated with DNA damage repair and radiosensitivity in CRC cells. *Lnc-RI* via competitive binding of miR-4727-5p regulates *LIG4* expression to participate in DNA damage repair, affecting cell cycle and radiosensitivity (Fig. 6). We show that *lnc-RI* represents an important CRC therapeutic target whose knockdown can inhibit the DNA damage repair ability of tumor cells, promoting tumor cell death in combination with antitumor drugs or/and radiation therapy.

**Compliance with ethical standards**

**Ethical approval and consent to participate**   Animal experiments were approved by the ethics committee of the Animal Center of Beijing Institute of Radiation Medicine. Clinical samples have been reviewed and approved by the Ethics Committee of Liaoning Cancer Hospital (20190970).

**Competing interests**   The authors declare that they have no competing interests.

## References

Adlakha YK, Saini N. Brain microRNAs and insights into biological functions and therapeutic potential of brain enriched miRNA-128. Mol Cancer. 2014;13:33.

Baker B, Salameh H, Al-Salman M, Daoud F. How does preoperative radiotherapy affect the rate of sphincter-sparing surgery in rectal cancer? Surg Oncol. 2012;21(3):e103–9.

Barshishat S, Elgrably Weiss M, Edelstein J, Georg J, Govindarajan S, Haviv M, et al. OxyS small RNA induces cell cycle arrest to allow DNA damage repair. EMBO J. 2018;37(3):413–26.

Bartlett EJ, Brissett NC, Plocinski P, Carlberg T, Doherty AJ. Molecular basis for DNA strand displacement by NHEJ repair polymerases. Nucleic Acids Res. 2016;44(5):2173–86.

Chang HHY, Pannunzio NR, Adachi N, Lieber MR. Non-homologous DNA end joining and alternative pathways to double-strand break repair. Nat Rev Mol Cell Biol. 2017;18(8):495–506.

Chen X, Chen Z, Yu S, Nie F, Yan S, Ma P, et al. Long noncoding RNA LINC01234 functions as a competing endogenous RNA to regulate CBFB expression by sponging miR-204-5p in gastric cancer. Clin Cancer Res. 2018;24(8):2002–14.

Chen S, Liu R, Wang Q, Qi Z, Hu Y, Zhou P, et al. MiR-34s negatively regulate homologous recombination through targeting RAD51. Arch Biochem Biophys. 2019;666:73–82.

Conlin MP, Reid DA, Small GW, Chang HH, Watanabe G, Lieber MR, et al. DNA ligase IV guides end-processing choice during nonhomologous end joining. Cell Rep. 2017;20:2810–9.

Coutelier H, Xu Z, Morisse MC, Lhuillier-Akakpo M, Pelet S, Charvin G, et al. Adaptation to DNA damage checkpoint in senescent telomerase-negative cells promotes genome instability. Genes Dev. 2018;32(23–24):1499–513.

Dai L, Liu Y, Liu J, Wen X, Xu Z, Wang Z, et al. A novel CyclinE/CyclinA-CDK inhibitor targets p27Kip1 degradation, cell cycle progression and cell survival: implications in cancer therapy. Cancer Lett. 2013;333(1):103–12.

Davidovich C, Cech TR. The recruitment of chromatin modifiers by long noncoding RNAs: lessons from PRC2. RNA. 2015;21(12):2007–22.

Dianatpour A, Ghafouri-Fard S. The role of long non coding RNAs in the repair of DNA double strand breaks. Int J Mol Cell Med. 2017;6(1):1–12.

Foster SS, De S, Johnson LK, Petrini JHJ, Stracker TH. Cell cycle- and DNA repair pathway-specific effects of apoptosis on tumor suppression. Proc Natl Acad Sci. 2012;109(25):9953–8.

Furió-Tarí P, Tarazona S, Gabaldón T, Enright AJ, Conesa A. spongeScan: a web for detecting microRNA binding elements in lncRNA sequences. Nucleic Acids Res. 2016;44(W1):W176–80.

Giraldez MD, Spengler RM, Etheridge A, Goicochea AJ, Tuck M, Choi SW, et al. Phospho-RNA-seq: a modified small RNA-seq method that reveals circulating mRNA and lncRNA fragments as potential biomarkers in human plasma. EMBO J. 2019;38(11):e101695.

Goldstein M, Kastan MB. The DNA damage response: implications for tumor responses to radiation and chemotherapy. Annu Rev Med. 2015;66(1):129–43.

Hatano K, Kumar B, Zhang Y, Coulter JB, Hedayati M, Mears B, et al. A functional screen identifies miRNAs that inhibit DNA repair and sensitize prostate cancer cells to ionizing radiation. Nucleic Acids Res. 2015;43(8):4075–86.

Jiang N, Shen Y, Fei X, Sheng K, Sun P, Qiu Y, et al. Valosin-containing protein regulates the proteasome-mediated degradation of DNA-PKcs in glioma cells. Cell Death Dis. 2013;4(5):e647.

Jiang Y, Jiang Y, Xie J, Mayakonda A, Hazawa M, Chen L, et al. Co-activation of super-enhancer-driven CCAT1 by TP63 and SOX2 promotes squamous cancer progression. Nat Commun. 2018;9(3619).

Katyal S, Lee Y, Nitiss KC, Downing SM, Li Y, Shimada M, et al. Aberrant topoisomerase-1 DNA lesions are pathogenic in neurodegenerative genome instability syndromes. Nat Neurosci. 2014;17(6):813–21.

Kawai K, Ishihara S, Nozawa H, Hata K, Kiyomatsu T, Morikawa T, et al. Prediction of pathological complete response using endoscopic findings and outcomes of patients who underwent watchful waiting after chemoradiotherapy for rectal cancer. Dis Colon Rectum. 2017;60(4):368–75.

Li XL, Subramanian M, Jones MF, Chaudhary R, Singh DK, Zong X, et al. Long noncoding RNA PURPL suppresses basal p53 levels and promotes Tumorigenicity in colorectal Cancer. Cell Rep. 2017;20(10):2408–23.

Lieber MR. The mechanism of double-strand DNA break repair by the nonhomologous DNA end-joining pathway. Annu Rev Biochem. 2010;79(1):181–211.

Lieber MR, Ma Y, Pannicke U, Schwarz K. Mechanism and regulation of human non-homologous DNA end-joining. Nat Rev Mol Cell Biol. 2003;4(9):712–20.

López-Otín C, Blasco MA, Partridge L, Serrano M, Kroemer G. The hallmarks of aging. Cell. 2013;153(6):1194–217.

Martens-Uzunova ES, Bottcher R, Croce CM, Jenster G, Visakorpi T, Calin GA. Long noncoding RNA in prostate, bladder, and kidney cancer. Eur Urol. 2014;65(6):1140–51.

Munschauer M, Nguyen CT, Sirokman K, Hartigan CR, Hogstrom L, Engreitz JM, et al. The NORAD lncRNA assembles a topoisomerase complex critical for genome stability. NATURE. 2018;561(7721):132–6.

Nurse P. The cell cycle, checkpoints, and cancer. Eur J Cancer. 1995;31:S135.

O'Driscoll M, Gennery AR, Seidel J, Concannon P, Jeggo PA. An overview of three new disorders associated with genetic instability: LIG4 syndrome, RS-SCID and ATR-Seckel syndrome. DNA Repair. 2004;3(25):1227–35.

Pounami Samaddera B, Rakesh Aithala C, Belanc O, Krejci L. Cancer TARGETases DSB repair as a pharmacological target. Pharmacol Ther. 2016;161:111–31.

Ren S, Peng Z, Mao JH, Yu Y, Yin C, Gao X, et al. RNA-seq analysis of prostate cancer in the Chinese population identifies recurrent gene fusions, cancer-associated long noncoding RNAs and aberrant alternative splicings. Cell Res. 2012;22(5):806–21.

Rube CE, Grudzenski S, Kuhne M, Dong X, Rief N, Lobrich M, et al. DNA double-strand break repair of blood lymphocytes and normal tissues analysed in a preclinical mouse model: implications for radiosensitivity testing. Clin Cancer Res. 2008;14(20):6546–55.

Sharma V, Khurana S, Kubben N, Abdelmohsen K, Oberdoerffer P, Gorospe M, et al. A BRCA1-interacting lncRNA regulates homologous recombination. EMBO Rep. 2015;16(11):1520–34.

Shen L, Wang Q, Liu R, Chen Z, Zhang X, Zhou P, et al. LncRNA lnc-RI regulates homologous recombination repair of DNA double-strand breaks by stabilizing RAD51 mRNA as a competitive endogenous RNA. Nucleic Acids Res. 2018;46(2):717–29.

Sole C, Arnaiz E, Manterola L, Otaegui D, Lawrie CH. The circulating transcriptome as a source of cancer liquid biopsy biomarkers. Semin Cancer Biol. 2019;58:100–8.

Spagnoletti G, Li BV, Piscazzi A, Giannelli F, Condelli V, Sisinni L, et al. Cyclin-dependent kinase 1 targeting improves sensitivity to radiation in BRAF V600E colorectal carcinoma cells. Tumour Biol. 2018;40(4).

Tarish FL, Schultz N, Tanoglidi A, Hamberg H, Letocha H, Karaszi K, et al. Castration radiosensitizes prostate cancer tissue by impairing DNA double-strand break repair. Sci Transl Med. 2015;7(312):312re11.

Thangavel C, Boopathi E, Ciment S, Liu Y, O'Neill R, Sharma A, et al. The retinoblastoma tumor suppressor modulates DNA repair and radioresponsiveness. Clin Cancer Res. 2014;20(21):5468–82.

Thapar R. Regulation of DNA double-strand break repair by non-coding RNAs. Molecules. 2018;23(11):2789.

Urick ME, Chung EJ, Shield WP, Gerber N, White A, Sowers A, et al. Enhancement of 5-fluorouracil-induced in vitro and in vivo radiosensitization with MEK inhibition. Clin Cancer Res. 2011;17(15):5038–47.

Wang Z, Shen L, Chang C, Zhang X, Chen Z, Li L, et al. Long noncoding RNA lnc-RI is a new regulator of mitosis via targeting miRNA-210-3p to release PLK1 mRNA activity. Sci Rep-Uk. 2016;6(25385).

Wang X, Liu H, Shi L, Yu X, Gu Y, Sun X. LINP1 facilitates DNA damage repair through non-homologous end joining (NHEJ) pathway and subsequently decreases the sensitivity of cervical cancer cells to ionizing radiation. Cell Cycle. 2018;17(4):439–47.

Yu H, Xu Q, Liu F, Ye X, Wang J, Meng X. Identification and validation of long noncoding RNA biomarkers in human non–small-cell lung carcinomas. J Thorac Oncol. 2015;10(4):645–54.

Zhang Y, He Q, Hu Z, Feng Y, Fan L, Tang Z, et al. Long noncoding RNA LINP1 regulates repair of DNA double-strand breaks in triple-negative breast cancer. Nat Struct Mol Biol. 2016;23(6):522–30.

Zhao Y, Liu Y, Lin L, Huang Q, He W, Zhang S, et al. The lncRNA MACC1-AS1 promotes gastric cancer cell metabolic plasticity via AMPK/Lin28 mediated mRNA stability of MACC1. Mol Cancer. 2018;17(69).

Zhu M, Liu J, Xiao J, Yang L, Cai M, Shen H, et al. Lnc-mg is a long non-coding RNA that promotes myogenesis. Nat Commun. 2017;8(14718).